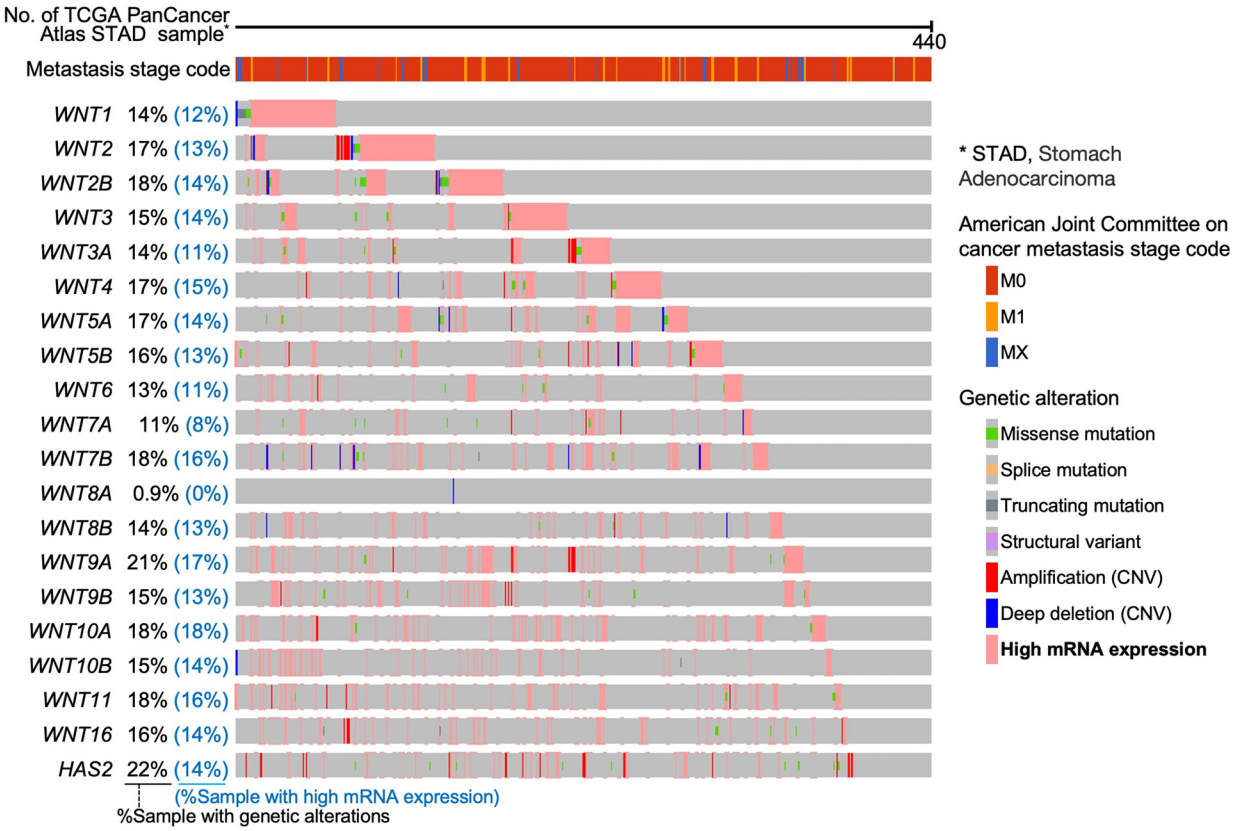

Supplementary Figure 1

Genetic alterations in WNT ligand family genes across 440 stomach adenocarcinoma (STAD) samples from the TCGA PanCancer Atlas using the cBioPortal database. The data include missense mutations, splice mutations, truncating mutations, structural variants, copy number gains (amplifications), copy number losses (deep deletions), and mRNA overexpression. mRNA overexpression was defined by Z-scores (log-transformed) of ≥1, based on comparison to the expression distribution across samples. A total of 361 out of 440 samples met this criterion for *WNTs* or *HAS2*. The distribution of genetic alterations was visualized using OncoPrint plot. Metastasis stages are indicated by color: M0 (red), M1 (orange), and MX (blue). Source Data are provided as a Source Data file.

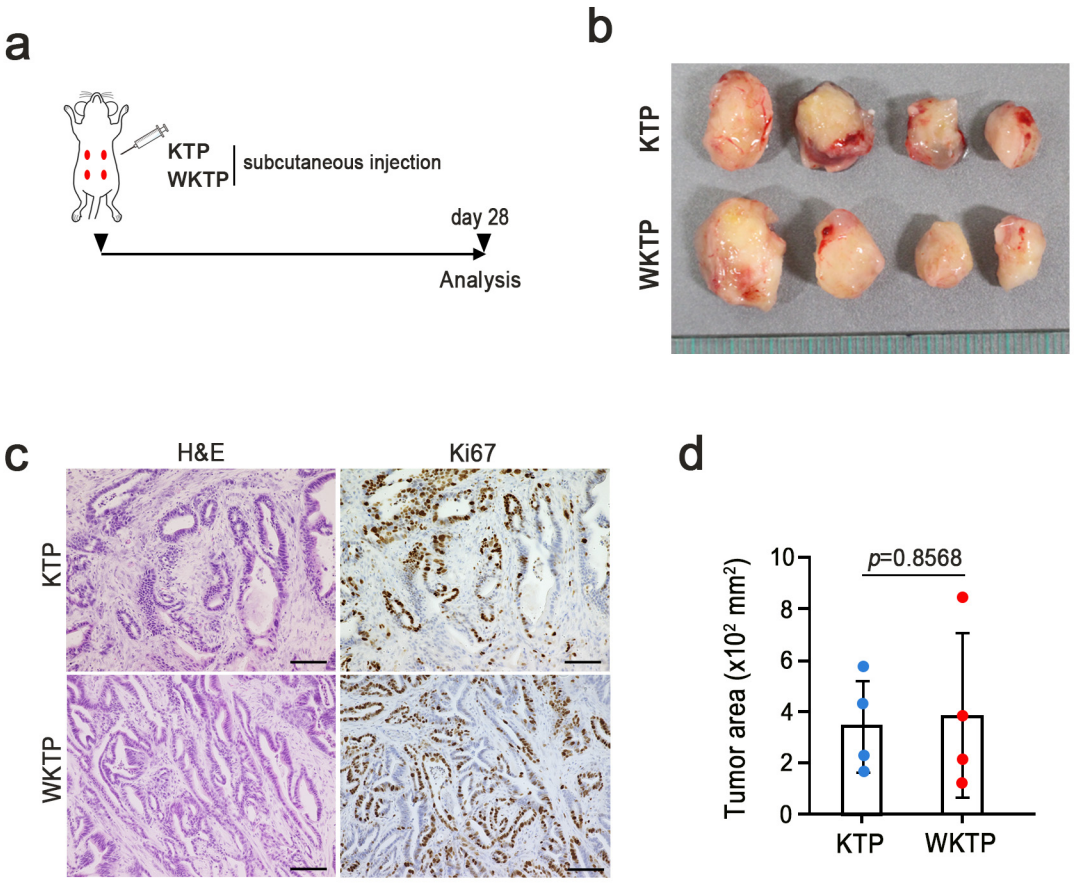

Supplementary Figure 2

Subcutaneous (*s.c.*) tumor formation by KTP and WKTP cells. (a) Graphic overview of the organoid subcutaneous (*s.c.*) transplantation experiments. (b) Representative macroscopic images of *s.c.* tumors formed by KTP and WKTP cells from *n*=3 biologically independent animals for each genotype. (c) Representative histological images of H&E staining and Ki67 immunohistochemistry of KTP and WKTP *s.c.* tumors. Bars, 100 μm. The photographs are representative images from *n*=3 biological independent animals for each genotype. (d) Tumor area measurements based on histological sections, presented as a bar graph (*n*=4 biologically independent samples for each genotype) (mean ± s.d.). A two-sided unpaired *t*-test was used to calculate statistical significance. *P* value is provided. Source data are provided as a Source Data file.

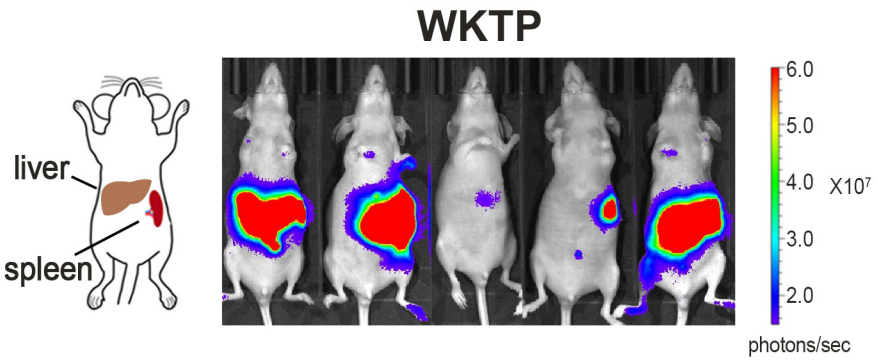

Supplementary Figure 3

The *in vivo* imaging photographs for transplanted WKTP organoid-derived tumors at 28 days after transplantation are shown (orthotopic transplantation; *n*=5 biologically independent mice). Color scale bar indicates intensity of luminescence. The liver and spleen areas are indicated on the left. Note that three of five mice exhibit peritoneal dissemination.

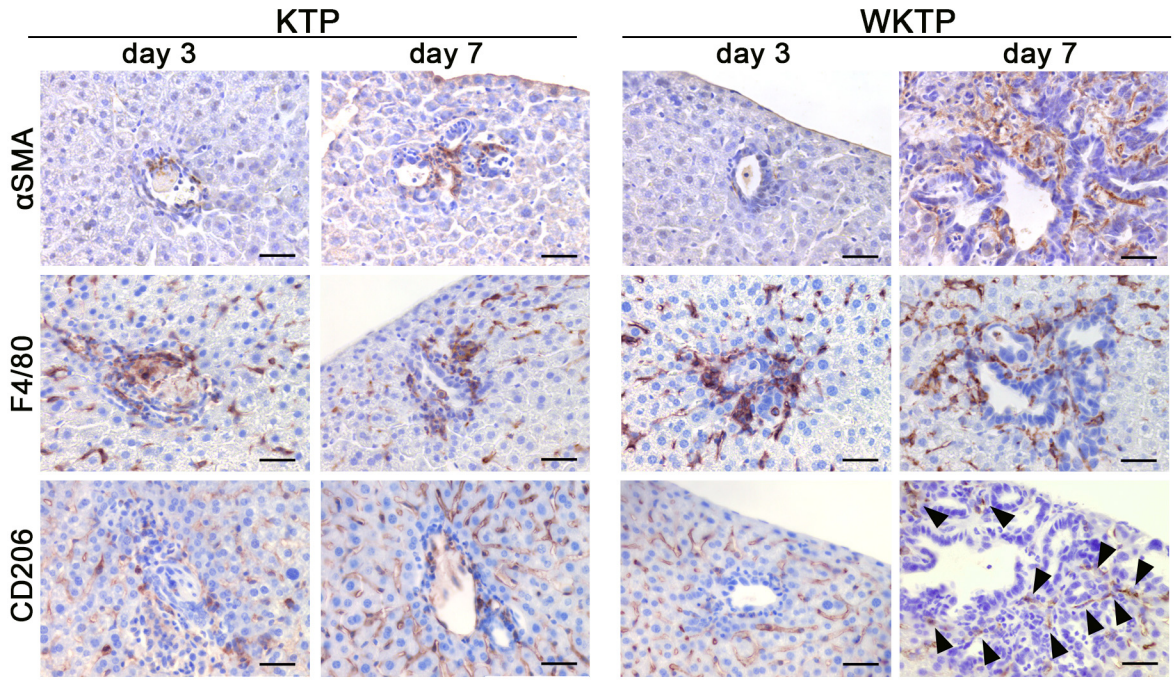

Supplementary Figure 4

Tumor microenvironment during the early stage of metastatic tumor development. Representative immunostaining images for αSMA (top), F4/80 (middle), and CD206 (bottom) in the livers of mice transplanted with KTP or WKTP organoids, examined at day 3 and day 7 after intrasplenic injection. Bars, 30 μm. The photographs are representative images (*n*=3 biologically independent animals for each genotype). Arrowheads indicate CD206 positive M2 macrophages in WKTP tumors at day 7.

a

Apc gene exon 3

TCCCTTCGCTCCTACGGAAGTCGGGAAGGATCTGTATCCAGCCGTTCAGG

gRNA

b

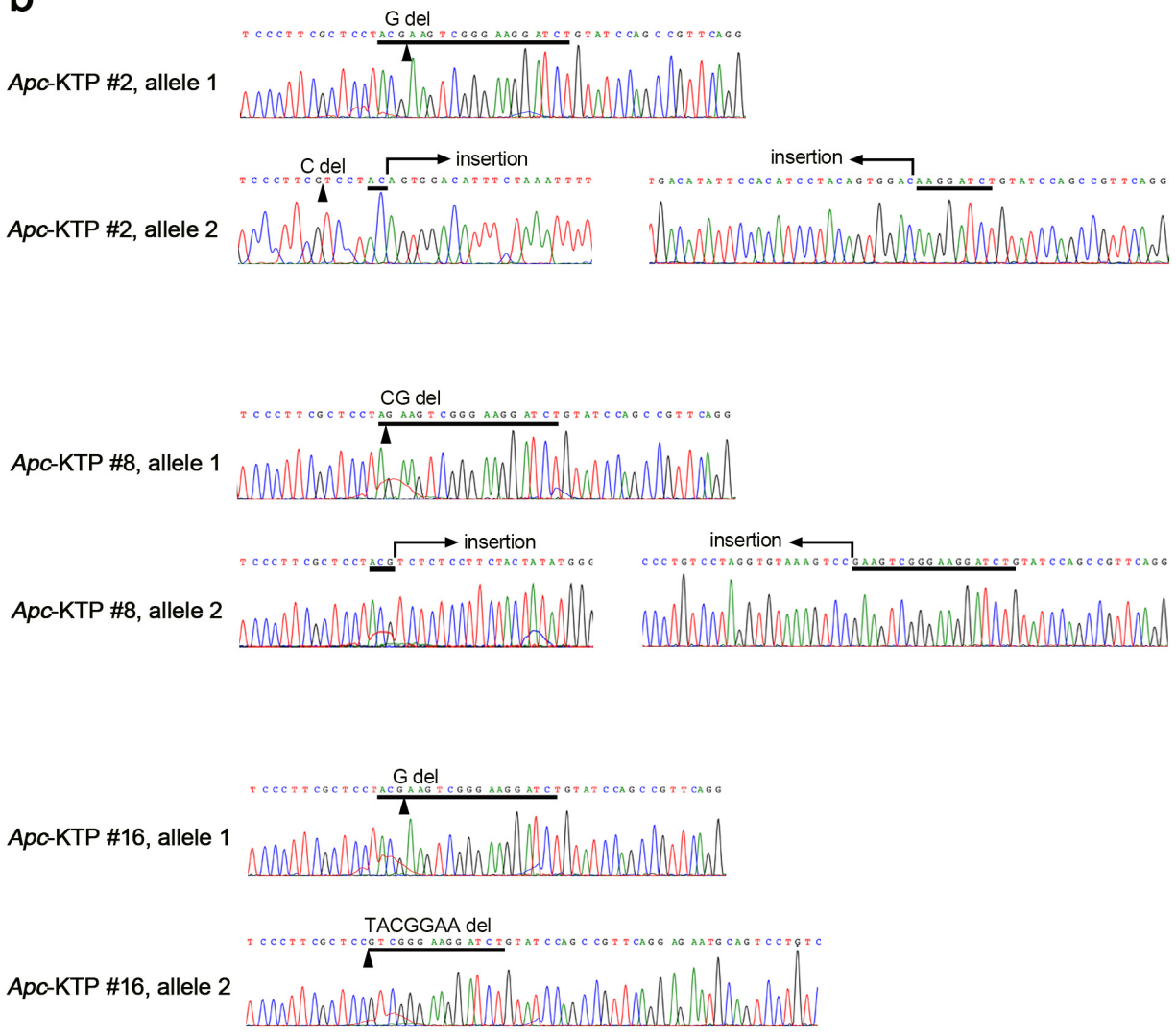

Supplementary Figure 5

Validation of *Apc* gene disruption in KTP organoid cells by genomic sequencing. (a) Guide RNA (gRNA) sequence targeting exon 3 of mouse *Apc* gene. (b) Representative sequencing results showing mutations around the gRNA target site in both alleles from three independent *Apc*-KTP organoid lines.

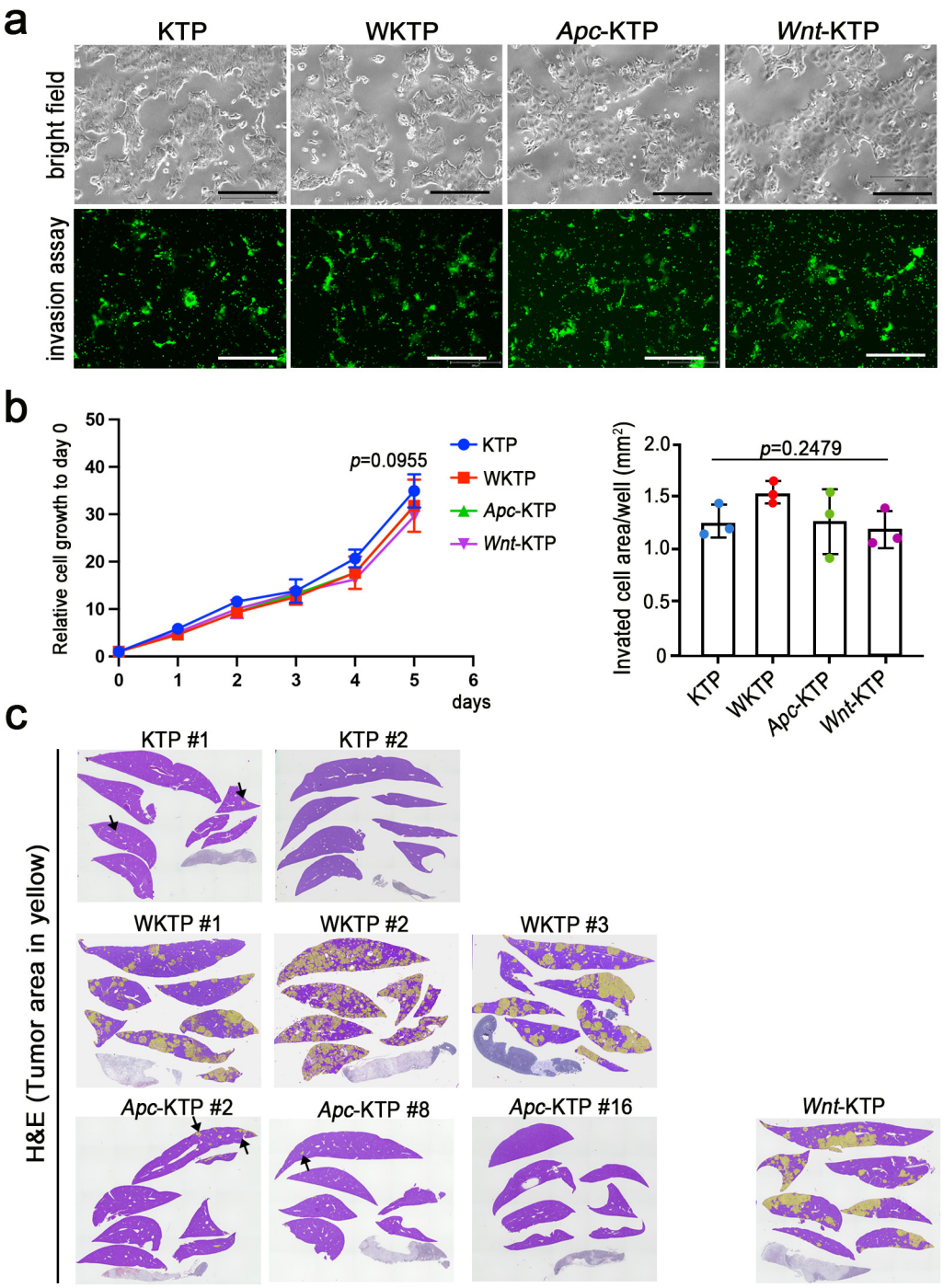

Supplementary Figure 6

In vitro and *in vivo* analyses of *Apc*-KTP and *Wnt*-KTP cells. (a) Representative images of cell morphology (top) and invasion assay (bottom) for KTP, WKTP, *Apc*-KTP, and *Wnt*-KTP cells. Bars, 300 μm. (b) Results of CTG cell proliferation assay (left) (n=8 biologically independent samples for KTP, WKTP, and *Apc*-KTP, and n=4 for *Wnt*-KTP) and invasion assay (right) (n=3 biologically independent samples for each genotype) are indicated as mean ± s.d. One-way ANOVA followed by Turkey's post-hoc test was used to calculate statistical significance. P values are provided. Source data are provided as a Source Data file. (c) Representative images of livers from mice transplanted with KTP (top), WKTP (middle), *Apc*-WKTP, and *Wnt*-KTP cells (bottom). Tumor areas are highlighted in yellow. Arrows indicate small tumor cell clusters in KTP and *Apc*-KTP cells. The photographs in a and c are representative images from n=3 independent culture experiments and n=3 biologically independent animals, respectively, for each genotype.

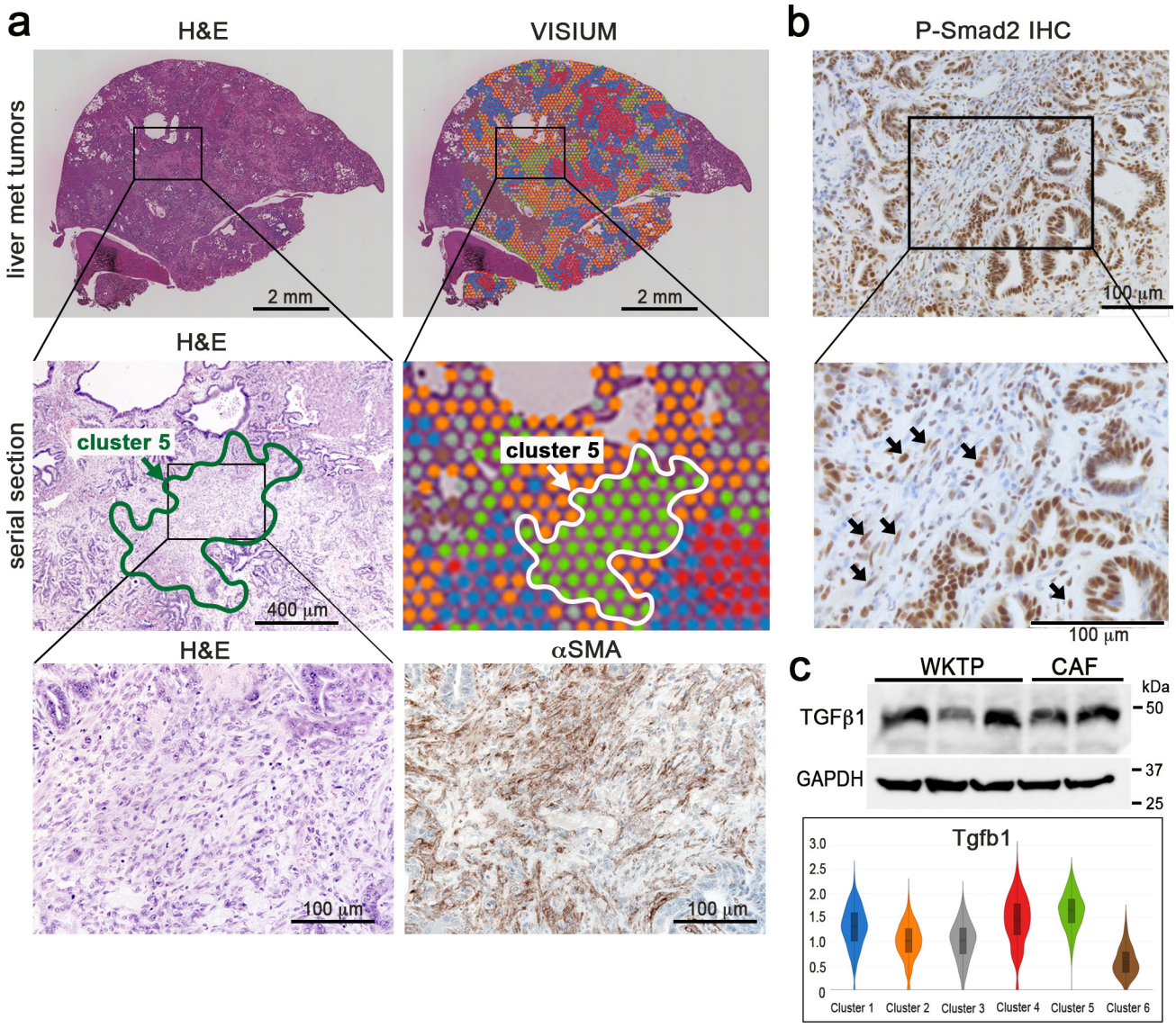

Supplementary Figure 7

Enrichment of cancer-associated fibroblasts (CAFs) in cluster 5. (a) H&E staining and Visium spatial transcriptomics analysis of liver metastatic tumors of WKTP cells (top), with enlarged images of the boxed areas (middle) are shown. Cluster 5 regions are outlined in green or white. Representative images of H&E and αSMA immunohistochemistry of cluster 5 are shown (bottom). Scale bars are included. (The same H&E staining and Visium data shown in Fig. 5B). (b) Representative immunohistochemistry images for phosphorylated Smad2 (P-Smad2) in WKTP cell liver metastasis. Arrows indicate stromal cells exhibiting nuclear accumulation of P-Smad2. Scale bars are included. The photographs are representative images from *n*=3 biologically independent animals. (c) Immunoblotting analysis of TGFβ1 expression in WKTP and CAFs, with GAPDH as an internal control (*n*=3 biologically independent samples for WKTP, and *n*=2 for CAFs) (top). Molecular weight markers (kDa) are provided. Violin plots showing *Tgfb1* expression across spatial clusters are shown (bottom). Boxes indicate the interquartile range (25th-75th percentiles), center lines indicate the median, and whiskers indicate the minimum and maximum values. Source data are provided as a Source Data file.

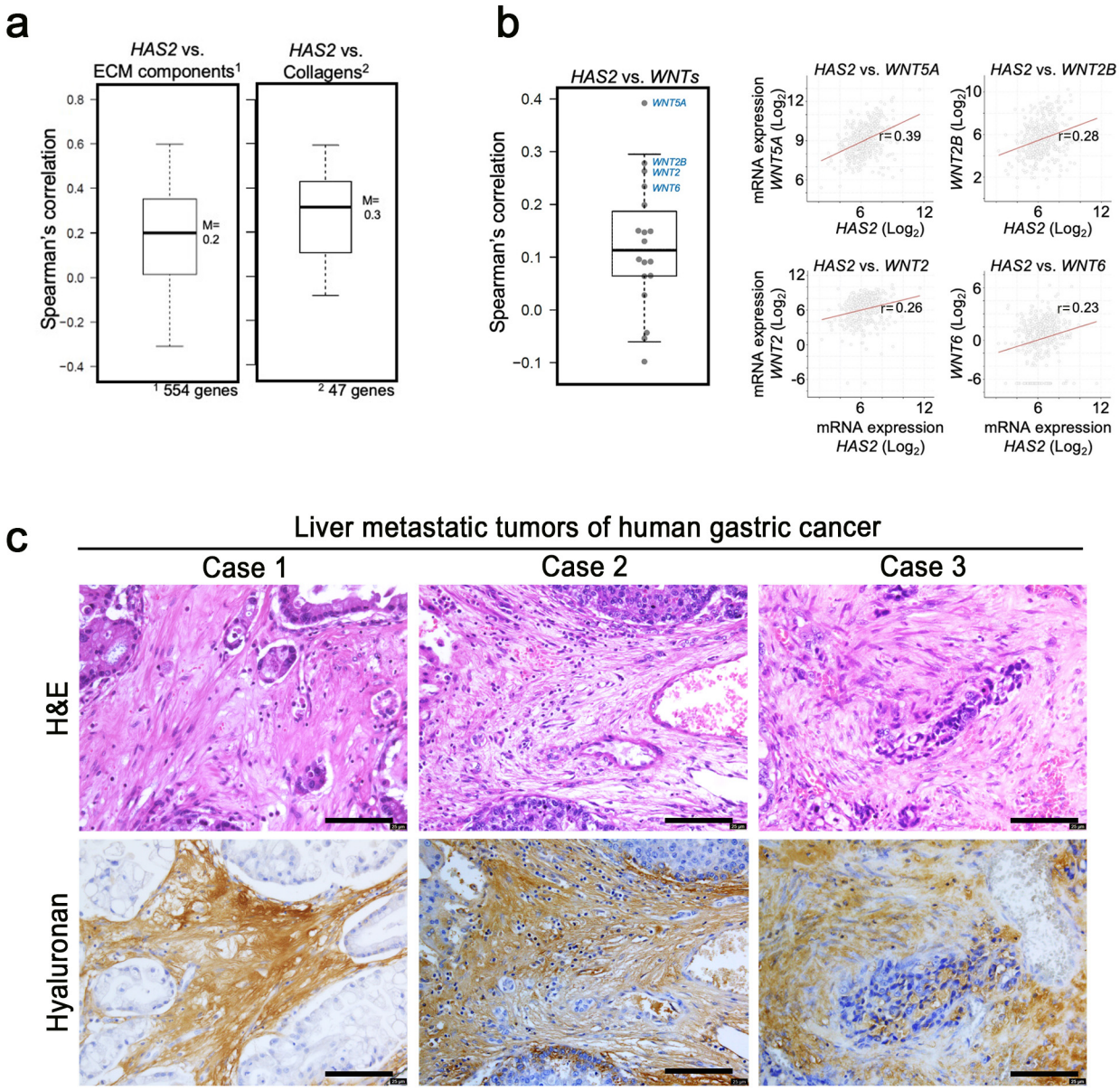

Supplementary Figure 8

HAS2 expression and hyaluronan deposition in human gastric cancer. (a) Correlation analysis between *HAS2* expression and ECM component-related genes (left) or collagen family genes (right) in human gastric cancer. Co-expression analysis was conducted using cBioPortal based on 440 STAD (stomach adenocarcinoma) samples from the TCGA database, using Spearman's correlation. (b) Correlation analysis between expression of *HAS2* and the *WNT* family genes (left). Spearman's rank correlation was used to assess the association between *HAS2* expression and *WNT5A*, *WNT2B*, *WNT2*, or *WNT6* expression (right). Spearman's ρ values are provided. In the box plot in panels a and b, boxes show the interquartile range (25th-75th percentiles), the center line indicates the median (M). (c) Representative histological images of H&E staining (top) and biotinylated hyaluronan probe staining (bottom). The photographs are representative images from *n*=3 independent human gastric cancer liver metastasis samples. Bars, 100 μm. Source data for a and b are provided as a Source Data file.

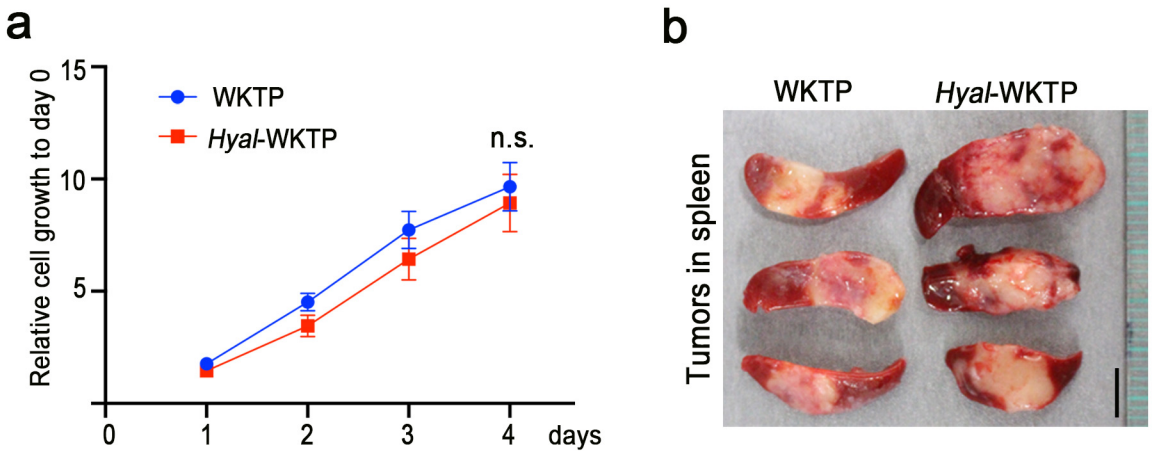

Supplementary Figure 9
Tumor development of *Hyal*-WKTP cells in the spleen. (a) Cell proliferation of WKTP and *Hyal*-WKTP cells assessed by CTG assay (*n*=8 biologically independent samples for each genotype). Results are presented as a line graph (mean ± s.d.). A two-sided unpaired *t*-test was used to calculate statistical significance at day 4. *P* value is provided. Source data are provided as a Source Data file. (b) The macroscopic images of spleens showing tumor development following intrasplenic transplantation of WKTP and *Hyal*-WKTP cells (*n*=3 biologically independent animals for each genotype organoid). Bars, 5 mm.

Genotype*	Mouse primary tumors in the stomach		Genotype
	Gastric mucosa	Submucosa	
K	Hyperplasia & metaplasia	No tumor	K
KT	Hyperplasia & metaplasia	Invasive tumor	KT
KP	Hyperplasia & metaplasia	No tumor	KP
KTP	Hyperplasia & metaplasia	Invasive tumor	KTP
WKT	Dysplastic tumor	Invasive tumor	WKT
WKP	Dysplastic tumor	No tumor	WKP
WKTP	Dysplastic tumor	Invasive tumor	WKTP

*Mouse genotype information

W *K19-Wnt1*
K *Kras*$^{+/G12D}$
KT *Kras*$^{+/G12D}$ *Tgfbr2*$^{-/-}$
KP *Kras*$^{+/G12D}$ *Trp53*$^{+/R270H}$
KTP *Kras*$^{+/G12D}$ *Tgfbr2*$^{-/-}$ *Trp53*$^{+/R270H}$
WKT *K19-Wnt1 Kras*$^{+/G12D}$ *Tgfbr2*$^{-/-}$
WKP *K19-Wnt1 Kras*$^{+/G12D}$ *Trp53*$^{+/R270H}$
WKTP *K19-Wnt1 Kras*$^{+/G12D}$ *Tgfbr2*$^{-/-}$ *Trp53*$^{+/R270H}$

Supplementary Table 1
Histological characteristics of the glandular stomach in various genetically engineered mouse models. *Kras* mutation without *Wnt1* expression (K, KT, KP, and KTP) induces epithelial hyperplasia and metaplasia in the gastric mucosa. In contrast, the addition of *Wnt1* expression (WKT, WKP, and WKTP) promotes the development of dysplastic tumors. Models harboring both *Kras* and *Tgfbr2* mutations (KT, KTP, WKT, and WKTP) exhibit submucosal invasion.
*Mouse genotypes are provided.